


Origin of the vortex displacement field in twisted bilayer graphene

Yu. N. Gornostyrev^{1,2} and M. I. Katsnelson^{3,2}

¹*M. N. Mikheev Institute of Metal Physics UB RAS, S. Kovalevskaya Street 18, 620137 Ekaterinburg, Russia*

²*Ural Federal University, Mira Street 19, 620002 Ekaterinburg, Russia*

³*Institute for Molecules and Materials, Radboud University, NL-6525 AJ Nijmegen, The Netherlands*

 (Received 15 June 2020; revised 9 August 2020; accepted 10 August 2020; published 25 August 2020)

A model description of patterns of atomic displacements in twisted bilayer systems has been proposed. The model is based on the consideration of several dislocation ensembles, employing a language that is widely used for grain boundaries and film/substrate systems. We demonstrate explicitly how the dislocation language relates to vortex lattice motives found in experiment and simulations. We show that three ensembles of parallel screw dislocations are sufficient both to describe the rotation of the layers as a whole, and for the vortexlike displacements resulting from elastic relaxation. The results give a clear explanation of the observed features of the structural state such as vortices, accompanied by alternating stacking.

DOI: [10.1103/PhysRevB.102.085428](https://doi.org/10.1103/PhysRevB.102.085428)

I. INTRODUCTION

Bilayer systems consisting of two layers of identical or different two-dimensional materials such as bilayer graphene (G/G), bilayer hexagonal boron nitride (BN/BN), and bilayer graphene/hexagonal boron nitride (G/BN) are the subject of great interest now as the simplest examples of van der Waals heterostructures (for reviews, see Refs. [1–3]). Building bilayer devices involves mechanical processes such as rotation and translation of one layer with respect to the other. This has substantial influence on the performance and quality of such devices [4,5]. The rotation leads to structural moiré patterns which directly affect the electronic properties of bilayers [6–14]. A further growth of interest in the field was triggered by a recent discovery of superconductivity and a metal-insulator transition in “magic angle” twisted bilayer graphene [15,16]. In this paper, we focus on the structural aspects of moiré patterns and consider bilayer G/G. We suggest a description of the moiré patterns in terms of vortices and in terms of dislocations and establish a connection between these two languages.

In two-dimensional materials, such as monolayer graphene, the term “dislocation” is typically used to describe pointlike [zero-dimensional (0D)] defects lying within the sheet, e.g., pentagon-heptagon or square-octagon pairs [17]; they are also used to describe grain boundaries as dislocation walls [18–20]. Such defects are edge dislocations with line directions oriented normal to the sheet. Unlike the case of monolayers, in bilayers it is also possible to have one-dimensional (line) dislocations that lie between the two layers of a bilayer material; these dislocations do not require the generation of any topological defects within each of two sheets.

The geometry of displacement fields in bilayer van der Waals systems has been discussed repeatedly starting from the discovery of a commensurate-incommensurate transition

in G/BN systems [10]. The results of atomistic simulations [21–23] show that the formation of the vortex lattice is rather typical for the picture of displacements of relaxed twisted bilayer systems (both G/BN and G/G). On the other hand, an electron microscopy study [24] revealed multiple stacking domains with solitonlike boundaries between them in slightly twisted bilayer graphene, where the domain boundaries can be also described as one-dimensional Frenkel-Kontorova dislocations, in which a topological defect where six domains meet can be considered as a vortex in a displacement field. A similar multiple stacking domain structure was discussed in Refs. [25,26] in the framework of a model employing a network of partial dislocation. However, the relation between these two descriptions, in terms of vortices and in terms of dislocations, is currently unclear.

Here, based on the dislocation model, we propose a general description of the moiré patterns in twisted bilayer graphene in terms of twisted grain boundaries in layered materials. We show that both pictures (vortex networks and dislocation arrays) are consistent and present two possible ways for a qualitative description of such systems and a physical interpretation of the computer simulation results.

II. DISLOCATION MODEL OF A TWISTED BILAYER SYSTEM

Moiré patterns are formed initially by a rigid twist of the upper layer with respect to the bottom layer; their geometry is determined by lattice type and the rotation angle [27]. If one allows atomic relaxation, that is, their shifts from these ideal geometric positions within the lattice of coincidence sites to minimize the total energy, the picture becomes more complicated and, according to simulations [22], a vortex displacement field arises. Notably, the vortices form a regular lattice and are separated by broad regions of almost zero displacements.

There are two canonical ways to describe conjugation in bilayer systems. The first one is the simplest picture of a coincidence site lattice (CSL) [28], where one lattice is just rotated and placed on the other one without atomic relaxation; it corresponds to the moiré description. In the second approach, a general description of twist boundaries in bilayer systems can be derived on the basis of dislocation models proposed earlier for three-dimensional materials and thin films [29]. A consideration of grain boundaries based on the concept of surface dislocations was given in Ref. [30] where general relations between grain boundaries and the geometry of dislocation arrays were discussed. In the context of graphene, this language was used in Refs. [18–20].

A. General geometric relationships

At least two arrays of parallel equidistant screw dislocations are necessary to ensure a given relative twist of two crystallites in their conjugation plane [30]. In this case, certain geometric relations must be fulfilled so that the total shear deformation in the plane of the boundary is zero. In particular, in the case of two arrays, it is necessary to require that the dislocation axes in these arrays were perpendicular to each other.

To present correctly the geometry of the conjugation of two graphene layers (and the corresponding moiré pattern), two dislocation arrays are not enough. We consider a more general case and represent the plastic distortion tensor β_{ij}^p produced by one array of dislocations in the form $\beta_{ij}^p = n_i b_j / d$, where \mathbf{n} is the normal to the dislocation line lying in the plane of the boundary, \mathbf{b} is the Burgers vector of dislocation, and d is the distance between neighboring dislocations in the array. The plastic deformation ε_{ij}^p and rotation ω_{ij}^p are determined by the symmetric and antisymmetric parts of the tensor β_{ij}^p [30],

$$\varepsilon_{ij}^p = \frac{n_i b_j + n_j b_i}{2d}, \quad \omega_{ij}^p = \frac{n_i b_j - n_j b_i}{2d}. \quad (1)$$

To describe the conjugation of two twisted graphene layers and taking into account the lattice trigonal symmetry, we will use three dislocation arrays rotated with respect to each other by $\pi/3$. Assuming that the normal to the graphene layers is [001] and considering screw dislocations with the Burgers vector parallel to dislocation line, we write (see Fig. 1)

$$\begin{aligned} \mathbf{b}_1 &= b \left[\frac{\sqrt{3}}{2}, -\frac{1}{2}, 0 \right], & \mathbf{n}_1 &= \left[\frac{1}{2}, \frac{\sqrt{3}}{2}, 0 \right], \\ \mathbf{b}_2 &= b \left[\frac{\sqrt{3}}{2}, \frac{1}{2}, 0 \right], & \mathbf{n}_2 &= \left[-\frac{1}{2}, \frac{\sqrt{3}}{2}, 0 \right], \end{aligned} \quad (2)$$

where b is the module of the Burgers vector which should be equal to the elementary translation in the graphene layer. To ensure the total deformation ε_{ij}^p is equal to zero, it is necessary to choose the third dislocation array with the vector \mathbf{b}_3 orthogonal to $\mathbf{b}_1 + \mathbf{b}_2$,

$$\mathbf{b}_3 = b[0, 1, 0], \quad \mathbf{n}_3 = [-1, 0, 0]. \quad (3)$$

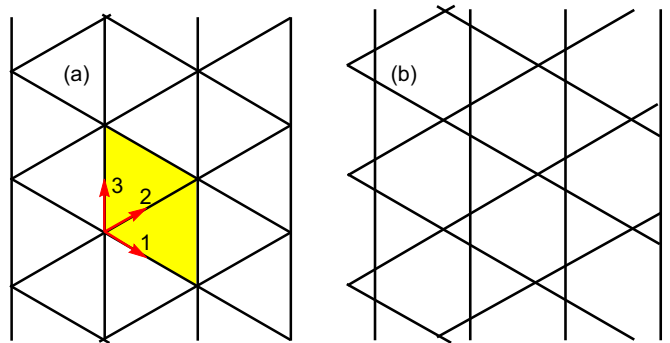


FIG. 1. The schematic representation of the dislocation network used to describe the twist boundary. (a) Network of screw dislocations. (b) Reconstructed network of dislocations. Vectors 1–3 indicate the directions of dislocation lines. The moiré cell is highlighted by a yellow tetragon.

Indeed, substituting expressions (2) and (3) into Eq. (1), we find

$$\varepsilon_{ij}^p = 0, \quad \omega_{ij}^p = \frac{3b}{2d} \begin{pmatrix} 0 & 1 & 0 \\ -1 & 0 & 0 \\ 0 & 0 & 0 \end{pmatrix}, \quad (4)$$

and the rotation vector $\omega_k = \frac{1}{2} \varepsilon_{ijk} \omega_{ij}$ will be $\omega = \frac{3b}{2d}[0, 0, 1]$. The periodicity of this dislocation network matches the period of the moiré picture and intersections of the dislocations correspond to the moiré coincidence points. Note that for a small rotation angle, $\psi \approx \omega_3 = 3b/(2d)$; this expression is similar to that determining the geometry of the moiré in the model of the CSL $\psi \sim a/l$, with l the distance between coincidence points, and a the elementary lattice translation.

B. Relaxed displacement field within the dislocation model

Equations (4) are valid on the average for the whole sheet. In fact, the displacements are nonuniformly distributed and concentrated near the dislocation lines. As discussed above, to describe correctly the displacement field in the case of twisted bilayer graphene, *three* arrays of dislocations are necessary. We believe that the Frenkel-Kontorova model [31] gives a qualitatively correct description of the displacement field created by surface dislocations. Assuming that the energy relief of the substrate may have an additional minimum [32,33] and dislocations can split into partial ones [30,31,34], the screw component of the displacement field for one family can be represented as

$$\begin{aligned} u_s(x) &= \frac{b}{\pi} \sum_i \left\{ \arctan \left[\exp \left(\frac{x - x_i^0 - \delta/2}{\xi} \right) \right] \right. \\ &\quad \left. + \arctan \left[\exp \left(\frac{x - x_i^0 + \delta/2}{\xi} \right) \right] \right\}, \end{aligned} \quad (5)$$

where x_i^0 correspond to the position of the center of dislocation line, ξ is the core width, $\delta \sim \mu b/\gamma$ is the distance splitting between partial dislocations, μ is the shear modulus, and γ is the stacking fault energy. A typical value of the core width is about a few lattice parameters a_0 [20]. As it was shown in Ref. [34], the splitting of total dislocations leads to

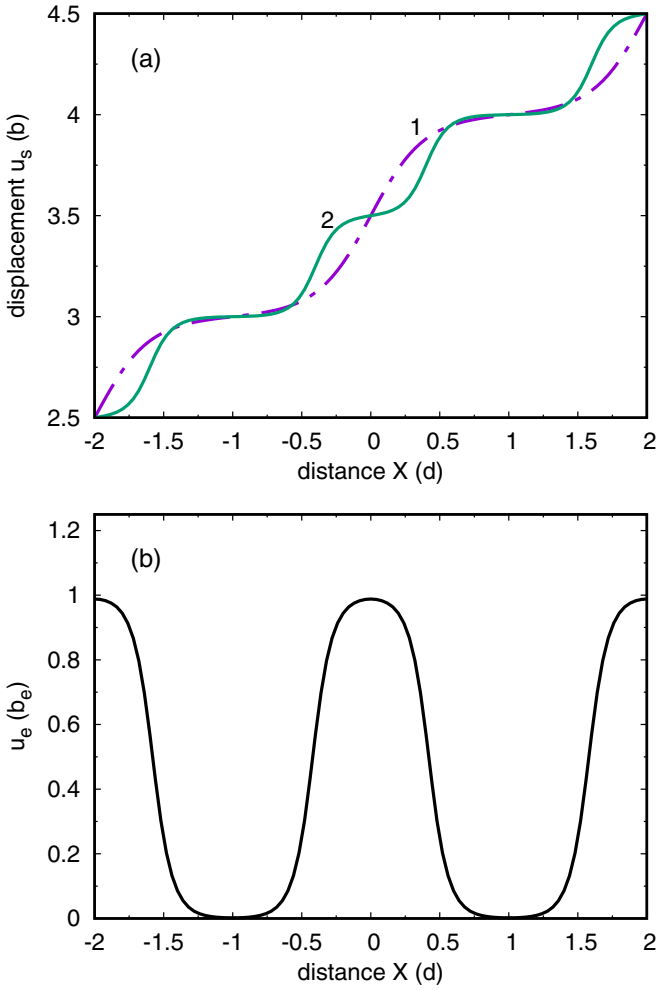


FIG. 2. Screw component (a) of displacements produced by one dislocation array in the case of nonsplit ($\xi = 0.2, \delta = 0.2$, curve 1) and split ($\xi = 0.1, \delta = 0.4$, curve 2) dislocation cores. Edge component (b) of the displacements is produced by one array of partial dislocation ($\xi = 0.1, \delta = 0.4$). Distances and parameters ξ, δ are given in units of d .

an AB-AC-AB alternation of stackings and results in a rather large distance between partial dislocations, about 20 nm.

The splitting of the dislocation on a hexagonal lattice results in the formation of a stacking fault which is accompanied also by the appearance of the edge components of partial dislocations [26], $\mathbf{b} = (\mathbf{b}/2 + \mathbf{b}_e) + (\mathbf{b}/2 - \mathbf{b}_e)$. In this case, the edge component of the displacement field can be written as

$$u_e(x) = \frac{b_e}{\pi} \sum_i \left\{ \arctan \left[\exp \left(\frac{x - x_i^0 - \delta/2}{\xi} \right) \right] - \arctan \left[\exp \left(\frac{x - x_i^0 + \delta/2}{\xi} \right) \right] \right\}. \quad (6)$$

Figure 2(a) displays the dependence $u_s(x)$ for the cases of narrow and wide (split) dislocations. In the case of narrow dislocations the displacements are concentrated in the dislocation core and include both plastic and elastic parts. When the width of the dislocation core ξ increases, the dependence

$u_s(x)$ becomes close to linear $u \approx u^p = bx/d$ and represents a pure plastic shear. Figure 2(b) shows the edge component of displacements in the case of split dislocation.

Following the discussion in the previous section, we represent the total displacement field in twisted graphene layers as a superposition of three dislocations arrays. Subtracting the plastic part, we write the elastic displacements produced by screw dislocations in the form

$$\mathbf{u}^{el}(\mathbf{r}) = \sum_{k=1}^3 \frac{\mathbf{b}_k}{\pi} \sum_{i=-m}^m \arctan \left[\exp \left(\frac{\mathbf{r}\mathbf{n}_k - x_i^k - \delta/2}{\xi} \right) \right] + \arctan \left[\exp \left(\frac{\mathbf{r}\mathbf{n}_k - x_i^k + \delta/2}{\xi} \right) \right] - \left(mb + \frac{b}{L} \mathbf{r}\mathbf{n}_k \right), \quad (7)$$

where $\mathbf{n}_k = [001] \times \mathbf{b}_k$ is the normal to the dislocation line of the k th array, $2m + 1$ is the number of dislocations in each array. In addition, in the case of split dislocations, there is a displacement field created by arrays of edge partial dislocations

$$\mathbf{u}_e(\mathbf{r}) = \sum_{k=1}^3 \frac{\mathbf{b}_k^p}{\pi} \sum_{i=-m}^m \left\{ \arctan \left[\exp \left(\frac{\mathbf{r}\mathbf{n}_k - x_i^k + \delta/2}{\xi} \right) \right] - \arctan \left[\exp \left(\frac{\mathbf{r}\mathbf{n}_k - x_i^k - \delta/2}{\xi} \right) \right] \right\}. \quad (8)$$

The vector fields described by Eq. (7) are shown in Fig. 3 for the cases of narrow (nonsplit) and split dislocation cores. As one can see from Figs. 3(a) and 3(c), the screw component of the displacement field produced by elastic relaxation (7) forms a vortex lattice. However, the geometry of displacements is quite different for the cases under consideration. In particular, dislocation splitting results in a decrease of the period of the vortex lattice by two times; the magnitude of displacement becomes essentially smaller [Fig. 3(c)]. The distribution of the edge components of the displacement field $\mathbf{u}_{edge}(\mathbf{r})$ [Fig. 3(d)] corresponds to alternating domains with almost constant displacements.

The picture of elastic displacement in Fig. 3(a) is rather similar to that obtained in atomistic simulations [22,33,35], which indicates a semiquantitative correctness of the description of atomic relaxation effects in twisted graphene bilayers within our simple dislocation model.

The distribution of the strain energy density [3]

$$E^{el} = \frac{1}{2} [\lambda (u_{\alpha\alpha})^2 + 2\mu u_{\alpha\beta} u_{\alpha\beta}] \quad (9)$$

is presented in Fig. 3(b). Here, the components of the deformation tensor are

$$\begin{aligned} u_{xx} &= \frac{du_x}{dx} + \frac{1}{2} \left(\frac{du_y}{dx} \right)^2 + \frac{1}{2} \left(\frac{du_x}{dy} \right)^2, \\ u_{yy} &= \frac{du_y}{dy} + \frac{1}{2} \left(\frac{du_x}{dy} \right)^2 + \frac{1}{2} \left(\frac{du_y}{dx} \right)^2, \\ u_{xy} &= \frac{1}{2} \left(\frac{du_x}{dy} + \frac{du_y}{dx} + \frac{du_x}{dy} \frac{du_x}{dx} + \frac{du_y}{dy} \frac{du_y}{dx} \right), \end{aligned} \quad (10)$$

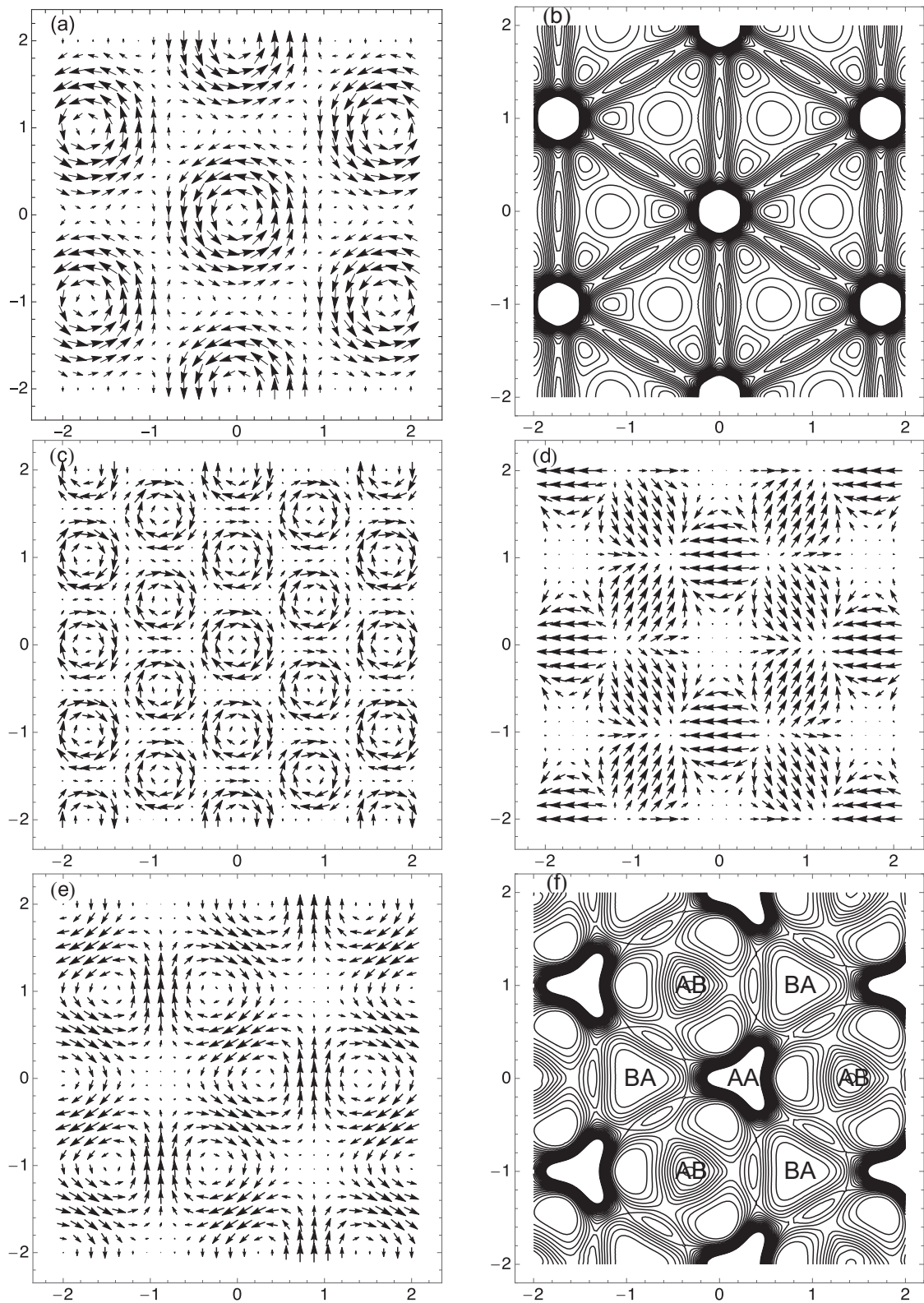


FIG. 3. Displacement $\mathbf{u}_{el}(\mathbf{r})$ shown as a vector field for (a) narrow and (c), (d) split dislocation cores ($\delta = 0.4d$), and (e) for the reconstructed dislocation network. (c) and (d) display screw and edge components of the displacement field, respectively, in the case of split dislocation. (b) and (f) present the distribution of the strain energy density determined by Eq. (9) for cases (a) and (e), respectively. The value ξ is equal $0.05d$ in cases (a)–(c) and $0.15d$ in cases (e) and (f). Distances along the X, Y axes are given in units of $L\sqrt{3}/2$, where L is the separation between the moiré coincidence points.

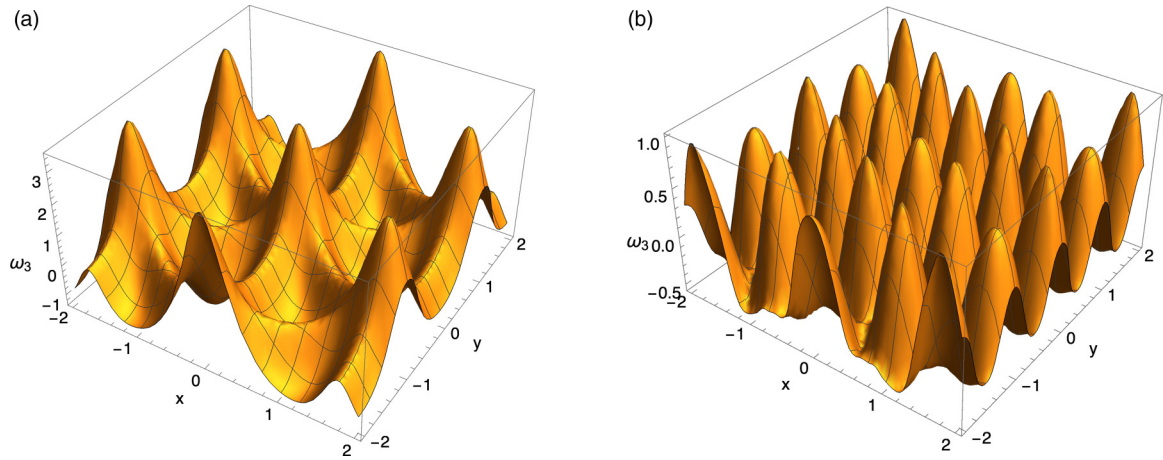


FIG. 4. Distribution of ω_3 , z component of the dimensionless rotation vector ω , for narrow (a) and split (b) dislocation cores. The corresponding displacement fields are shown in Figs. 3(a) and 3(c). Distances along the X, Y axes are given in units of $L\sqrt{3}/2$, where L is the separation between the moiré coincidence points.

and we take the ratio $\mu/\lambda = 5$, in agreement with the computational results for graphene [3]. Figure 3(b) shows that the elastic energy E^{el} is localized mostly near the dislocation lines. This picture agrees well with the results of atomistic simulations [35]. Although we considered complete dislocations when constructing Fig. 3(b), one should expect a similar distribution also for partial dislocations; in the latter case, they will separate areas with different stacking.

It is worthwhile to note that in the center of the vortex situated in the crossing of dislocation lines in Fig. 1, the relative displacement of the layers is equal to the half of the elementary translation which results in the formation of a stacking fault. In this case the more energetically favorable configuration is the one where one of the dislocation families is shifted from the symmetry position [Fig. 1(b)] by the value δl in the direction normal to the dislocation lines.

The distribution of the elastic displacements and strain energy after such a reconstruction of the dislocation network is shown in Figs. 3(e) and 3(f), respectively. One can see that the reconstruction of the dislocation network results in a drastic change of the displacement field $\mathbf{u}_{\text{el}}(\mathbf{r})$ [cf., Figs. 3(a) and 3(e)]. The primary vortices are centered at the AA-stacked regions and the secondary ones (in AB-stacked regions) originate from the overlap of the displacement field. According to Ref. [26], the structure of the layer conjugation in twisted bilayer graphene can be described in terms of a network of partial dislocations $a/3(1\bar{1}00)$ separating the regions of AB and BA stacking. The picture presented in Fig. 3(f) agrees qualitatively with that discussed in Ref. [26]; the density of elastic energy is concentrated near the lines of partial dislocation and in the area of their intersection the AA stacking is realized [25]. Note that the asymmetry of AB and BA stacking in Fig. 3(e) results from the limitations of the model considering three families of straight dislocations. Despite this shortcoming, our approach reproduces correctly the qualitative features of the layer conjugation.

The other quantity characterizing the peculiarities of the displacement field is the distribution of the rotation vector $\omega(\mathbf{r}) = \nabla \times \mathbf{u}_{\text{el}}(\mathbf{r})$ presented in Fig. 4. As one can see from this figure, in the case of a narrow core [Fig. 4(a)], the

dislocation lines are clearly visible in the distribution of the rotation vector and their intersections correspond to the centers of the vortices. At the same time, the only lattice of vortices remains visible in the case of split dislocations. Thus, depending on the representation used, the conjugation of layers can be described either in terms of vortices or dislocations, wherein the vortex displacement field originates naturally from the elastic relaxation of atomic positions. Note that the magnitude of the rotation vector ω is close to zero for the edge component of displacements.

The other characteristic which is actively discussed now [14] is the distribution of the pseudomagnetic field (PMF) [3,36] given by the equations

$$H_{\text{PMF}} = \frac{dA_y}{dx} - \frac{dA_x}{dy}, \quad (11)$$

where the vector potential is expressed (with the accuracy of some constant multiplier) via deformations as

$$A_x = u_{xx} - u_{yy}, \quad A_y = -2u_{xy}.$$

The distribution of PMF calculated from Eqs. (10) and (11) for the dislocation networks with the displacement field from Figs. 3(a) and 3(f) is shown in Fig. 5. The displacement field created by the network of narrow dislocations results in a regular alternation of triangular regions (left part of Fig. 5) with negative and positive values of the PMF; a similar distribution of PMF was obtained in the simulations [37]. The right-hand side of Fig. 5 shows the PMF distribution in the case of a reconstructed dislocation network. Pink regions (with negative PMF) correspond to the domains of small displacements in Fig. 3(d); quasicircular yellow regions with positive PMF are situated in between. The pictures presented here are characteristic of the flat dislocation network whereas out-of-plane deformations of the moiré pattern [14,38] can affect the distribution of PMF quite vitally.

III. DISCUSSION AND CONCLUSIONS

The model developed here allows us to explain naturally some qualitative peculiarities of the moiré patterns in bilayer

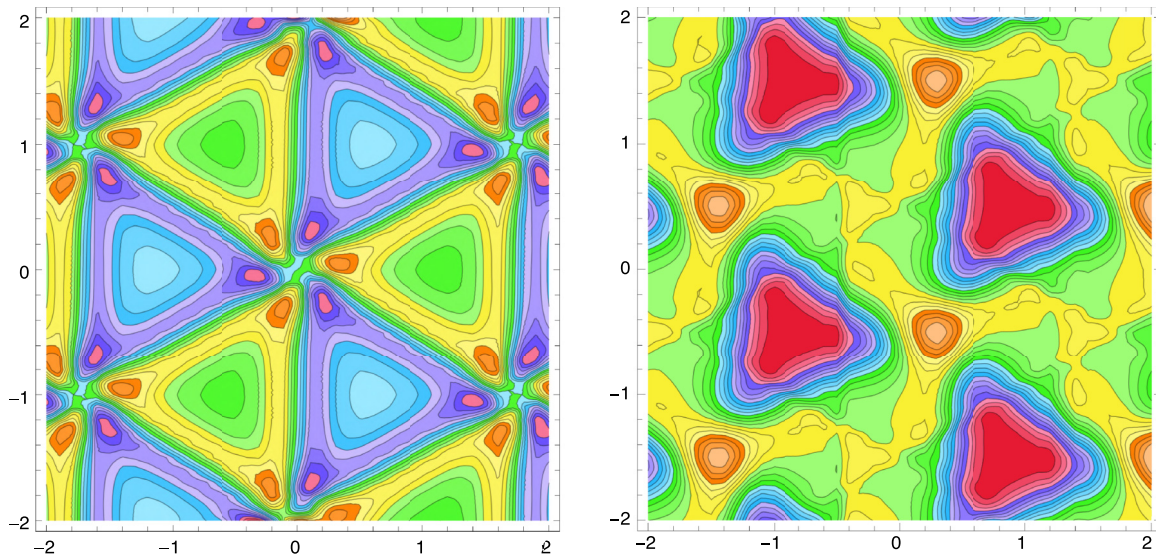


FIG. 5. Distribution of PMF calculated by using Eqs. (10) and (11) for the network of narrow dislocations shown in Fig. 3(a) (left) and for the reconstructed dislocation network shown in Fig. 3(e) (right). Distances along the X, Y axes are given in units of $L\sqrt{3}/2$, where L is the separation between the moiré coincidence points.

systems. In particular, the rotation angle and location of the coincidence site of the moiré patterns are related to the Burgers vector and the distance between dislocation lines (see Sec. II A). We show that the plastic part of the displacement field provides the rotation of one layer with respect to the other one as a whole. At the same time, the distribution of elastic displacements is quite complicated and vortices are the most typical elements; the observed picture is in qualitative agreement with both experiment [24] and the results of atomistic simulations [21–23,26].

Although, by construction, the displacements \mathbf{u}^{el} are equal to zero at a point located in the middle between two vortices, the derivative $du_i^{\text{el}}/dx_j \neq 0$. Note that the values du_i^{el}/dx_j depend on the distance between the dislocations in a given array and the width of their core. For narrow dislocations located far enough from each other, $du_i^{\text{el}}/dx_j \approx 0$ in the middle between two vortices. However, a more realistic consideration of the G/G case [26,32,33] assumes the dislocation core width is rather large, and the cores are situated close to each other. As a consequence, one should expect a remarkable deviation of the values du_i^{el}/dx_j from zero between the vortices. By using Eq. (7) and assuming $L \gg z$, we have $du_x^{\text{el}}/dx_y \approx 2b/\pi z \exp(-L/2z) \cosh(d/z)$. As a result, the region between the vortices is characterized by an excess of elastic energy density $\Delta E_{\text{el}} \sim \mu(du_x^{\text{el}}/dx_y)^2$. This additional energy can be reduced by the self-reorientation of the graphene layers [23] resulting in an increase in the distance between dislocations [cf., Eq. (4)].

Note that although the model does not take into account details related to the characteristics of chemical bonding, the formation of various types of stacking, and out-of-plane buckling, it provides a clear vision of the qualitative structural features of twisted bilayer systems. Our results unify the language used in the physics of moiré patterns in twisted bilayer graphene and other van der Waals heterostructures with that traditionally used for the description of nano- and mesostructures in solids. The proposed model gives a reasonable description of the structural features of twisted bilayer graphene, at least at not too large misorientation angles when the commensurate-incommensurate transition [10] occurs. The details of the chemical bonding enter our description via the model parameters, such as the width of the dislocation core ξ and the stacking fault energy γ . We suggest explicit analytical expressions for the distribution of atomic displacements in twisted bilayer graphene which can be used for both model theoretical studies and the interpretation of experimental and computational results.

ACKNOWLEDGMENTS

This work of M.I.K. was supported by the JTC-FLAGERA Project GRANSPOORT and the work of Y.N.G. was financed by the Russian Ministry of Education and Science (topic “Structure” A18-118020190116-6).

- [1] A. K. Geim and I. V. Grigorieva, *Nature (London)* **499**, 419 (2013).
 [2] Y. Liu, N. O. Weiss, X. Duan, H.-Ch. Cheng, Y. Huang, and X. Duan, *Nat. Rev. Mater.* **1**, 16042 (2016).

- [3] M. I. Katsnelson, *The Physics of Graphene*, 2nd ed. (Cambridge University Press, Cambridge, U.K., 2020).
 [4] G. Li, A. Luican, J. L. Dos Santos, A. Castro Neto, A. Reina, J. Kong, and E. Andrei, *Nat. Phys.* **6**, 109 (2009).

- [5] J. M. B. Lopes dos Santos, N. M. R. Peres, and A. H. Castro Neto, *Phys. Rev. Lett.* **99**, 256802 (2007).
- [6] W.-T. Pong and C. Durkan, *J. Phys. D* **38**, R329 (2005).
- [7] J. Xue, J. Sanchez-Yamagishi, D. Bulmash, P. Jacquod, A. Deshpande, K. Watanabe, T. Taniguchi, P. Jarillo-Herrero, and B. J. LeRoy, *Nat. Mater.* **10**, 282 (2011).
- [8] S. Tang, H. Wang, Y. Zhang, A. Li, H. Xie, X. Liu, L. Liu, T. Li, F. Huang, X. Xie, and M. Jiang, *Sci. Rep.* **3**, 2666 (2013).
- [9] W. Yang, G. Chen, Z. Shi, C.-C. Liu, L. Zhang, G. Xie, M. Cheng, D. Wang, R. Yang, D. Shi, K. Watanabe, T. Taniguchi, Y. Yao, Y. Zhang, and G. Zhang, *Nat. Mater.* **12**, 792 (2013).
- [10] C. R. Woods, L. Britnell, A. Eckmann, R. S. Ma, J. C. Lu, H. M. Guo, X. Lin, G. L. Yu, Y. Cao, R. V. Gorbachev, A. V. Kretinin, J. Park, L. A. Ponomarenko, M. I. Katsnelson, Yu. N. Gornostyrev, K. Watanabe, T. Taniguchi, C. Casiraghi, H.-J. Gao, A. K. Geim, and K. S. Novoselov, *Nat. Phys.* **10**, 451 (2014).
- [11] K. Uchida, Sh. Furuya, J.-I. Iwata, and A. Oshiyama, *Phys. Rev. B* **90**, 155451 (2014).
- [12] G. J. Slotman, M. M. van Wijk, P.-L. Zhao, A. Fasolino, M. I. Katsnelson, and S. Yuan, *Phys. Rev. Lett.* **115**, 186801 (2015).
- [13] P. Lucignano, D. Alfe, V. Cataudella, D. Ninno, and G. Cantele, *Phys. Rev. B* **99**, 195419 (2019).
- [14] H. Shi, Z. Zhan, Z. Qi, K. Huang, E. van Veen, J. A. Silva-Guillen, R. Zhang, P. Li, K. Xie, H. Ji, M. I. Katsnelson, S. Yuan, S. Qin, and Z. Zhang, *Nat. Commun.* **11**, 371 (2020).
- [15] Y. Cao, V. Fatemi, S. Fang, K. Watanabe, T. Taniguchi, E. Kaxiras, and P. Jarillo-Herrero, *Nature (London)* **556**, 43 (2018).
- [16] Y. Cao, V. Fatemi, A. Demir, S. Fang, S. L. Tomarken, J. Y. Luo, J. D. Sanchez-Yamagishi, K. Watanabe, T. Taniguchi, E. Kaxiras, R. C. Ashoori, and P. Jarillo-Herrero, *Nature (London)* **556**, 80 (2018).
- [17] D. R. Nelson, *Defects and Geometry in Condensed Matter Physics* (Cambridge University Press, Cambridge, U.K., 2002).
- [18] O. V. Yazyev and S. G. Louie, *Nat. Mater.* **9**, 806 (2010).
- [19] M. A. Akhukov, A. Fasolino, Y. N. Gornostyrev, and M. I. Katsnelson, *Phys. Rev. B* **85**, 115407 (2012).
- [20] S. Dai, Y. Xiang, and D. J. Srolovitz, *Phys. Rev. B* **93**, 085410 (2016).
- [21] M. M. van Wijk, A. Schuring, M. I. Katsnelson, and A. Fasolino, *Phys. Rev. Lett.* **113**, 135504 (2014).
- [22] M. M. van Wijk, A. Schuring, M. I. Katsnelson, and A. Fasolino, *2D Mater.* **2**, 034010 (2015).
- [23] C. R. Woods, F. Withers, M. J. Zhu, Y. Cao, G. Yu, A. Kozikov, M. Ben Shalom, S. V. Morozov, M. M. van Wijk, A. Fasolino, M. I. Katsnelson, K. Watanabe, T. Taniguchi, A. K. Geim, A. Mishchenko, and K. S. Novoselov, *Nat. Comm.* **7**, 10800 (2016).
- [24] J. S. Alden, A. W. Tsen, P. Y. Huang, R. Hovden, L. Brown, J. Park, D. A. Muller, and P. L. McEuen, *Proc. Natl. Acad. Sci. USA* **110**, 11256 (2013).
- [25] S. Hattendorf, A. Georgi, M. Liebmann, and M. Morgenstern, *Surf. Sci.* **610**, 53 (2013).
- [26] S. Bagchi, H. T. Johnson, and H. B. Chew, *Phys. Rev. B* **101**, 054109 (2020).
- [27] K. Hermann, *J. Phys.: Condens. Matter* **24**, 314210 (2012).
- [28] K. Sadananda and M. J. Marcinkowski, *J. Appl. Phys.* **45**, 1521 (1974).
- [29] R. Siems, P. Delavignette, and S. Amelinckx, *Phys. Status Solidi B* **2**, 421 (1962).
- [30] J. P. Hirth and J. Lothe, *Theory of Dislocations* (McGraw-Hill, New York, 1968).
- [31] O. M. Braun and Y. S. Kishvar, *The Frenkel-Kontorova Model: Concepts, Methods and Applications* (Springer, Berlin, 2004).
- [32] S. Zhou, J. Han, S. Dai, J. Sun, and D. J. Srolovitz, *Phys. Rev. B* **92**, 155438 (2015).
- [33] G. Savini, Y. J. Dappe, S. Öberg, J.-C. Charlier, M. I. Katsnelson, and A. Fasolino, *Carbon* **49**, 62 (2011).
- [34] B. Butz, C. Dolle, F. Niekel, K. Weber, D. Waldmann, H. B. Weber, B. Meyer, and E. Spiecker, *Nature (London)* **505**, 533 (2014).
- [35] S. K. Jain, V. Juri, and G. T. Barkema, *2D Mater.* **4**, 015018 (2017).
- [36] M. A. H. Vozmediano, M. I. Katsnelson, and F. Guinea, *Phys. Rep.* **496**, 109 (2010).
- [37] N. N. T. Nam and M. Koshino, *Phys. Rev. B* **96**, 075311 (2017).
- [38] M. Neek-Amal, P. Xu, D. Qi, P. M. Thibado, L. O. Nyakiti, V. D. Wheeler, R. L. Myers-Ward, C. R. Eddy, Jr., D. K. Gaskill, and F. M. Peeters, *Phys. Rev. B* **90**, 064101 (2014).